

In-beam tests of scintillating fibre detectors at MAMI and at GSI

P. Achenbach^{*}, C. Ayerbe Gayoso¹, J. C. Bernauer, R. Böhm,
M. O. Distler, L. Doria, M. Gómez Rodríguez de la Paz,
H. Merkel, U. Müller, L. Nungesser, J. Pochodzalla,
S. Sánchez Majos, B. S. Schlimme,
Th. Walcher, and M. Weinriefer

Institut für Kernphysik, Johannes Gutenberg-Universität, Mainz, Germany

L. Debenjak, M. Potokar, and S. Širca

University of Ljubljana and Jožef Stefan Institute, Ljubljana, Slovenia

M. Kavatsyuk, O. Lepyoshkina, S. Minami, D. Nakajima,
C. Rappold, T.R. Saito, D. Schardt, and M. Träger

GSI, Darmstadt, Germany

H. Iwase

KEK, Japan

S. Ajimura, A. Sakaguchi

Graduate School of Science, Osaka University, Japan

Y. Mizoi

*Division of Electronics and Applied Physics, Osaka Electro-Communication
University, Japan*

Abstract

The performance of scintillating fibre detectors was studied with electrons at the spectrometer facility of the Mainz microtron MAMI, as well as in a ^{12}C beam of 2 AGeV energy and in a beam of different particle species at GSI. Multi-anode photomultipliers were used to read out one or more bundles of 128 fibres each in different geometries. For electrons a time resolution of FWHM ~ 1 ns was measured in a single detector plane with a detection efficiency $\epsilon > 99\%$. A time resolution of

310 ps (FWHM) between two planes of fibres was achieved for carbon ions, leading to a FWHM ~ 220 ps for a single detector. The hit position residual was measured with a width of FWHM = 0.27 mm. The variation in the measured energy deposition was $\Delta E/E = 15\text{--}20\%$ (FWHM) for carbon ions. In addition, the energy response to $p/\pi^+/d$ particles was studied. Based on the good detector performance fibre hodoscopes will be constructed for the KAOS/A1 spectrometer at MAMI and for the HypHI experiment at GSI.

Key words: tracking and position-sensitive detectors, scintillating fibres, particle detector design

PACS: 29.40.Gx, 29.40.Mc, 85.60.Ha

1 Introduction

Detectors comprised of scintillating fibres that are packed together to form arrays and read out via multi-channel photo-detectors have been in use since the 1990s to track charged particles, e.g. [1; 2; 3].

At the Institut für Kernphysik in Mainz, Germany, the microtron MAMI has been upgraded to 1.5 GeV electron beam energy and can now be used to study strange hadronic systems. During the last years the KAOS/A1 spectrometer was installed with large angular acceptance under forward angles at the existing spectrometer facility for strangeness reaction spectroscopy. A large fibre detector set-up is under development for the KAOS/A1 spectrometer [4; 5; 6; 7]: the coordinate detector of the spectrometer's electron arm will consist of two vertical planes of fibre arrays, covering an active area of $L \times H \sim 1600 \times 300$ mm², supplemented by one or more horizontal planes.

The HypHI project is dedicated to hypernuclear spectroscopy with stable heavy ion beams and rare isotope beams at GSI, Germany, and FAIR, the Facility for Antiproton and Ion Research [8]. One of the central parts of the HypHI experiment is a scintillating fibre detector for the measurement of decay vertices of hypernuclei and for the tracking of charged particles directly behind the target. The fibre detector will also become crucial in distinguishing the hypernuclei ${}^4_{\Lambda}\text{H}$ and ${}^3_{\Lambda}\text{H}$ from the background containing α and Λ particles produced at the target. This detector is currently under development [9; 10].

In this paper results from beam-tests of scintillating fibre detectors are dis-

* Tel.: +49-6131-3925831; fax: +49-6131-3922964.

Email address: patrick@kph.uni-mainz.de (P. Achenbach).

¹ Part of doctoral thesis.

cussed. Section 2 describes the detectors and the read-out electronics. In Section 3 a resume of an investigation with electrons tracked through a large magnetic spectrometer at MAMI is given. The following Sections 3 and 4 show the results on position, time and energy resolutions obtained with primary ^{12}C beams and a beam of several particle species at GSI. Section 5 closes with the future prospects of using this kind of fibre detectors and electronics with the KAOS/A1 spectrometer at MAMI and within the HypHI project at GSI.

2 Detector geometries and read-out electronics

The fibres are of the standard (Non-S) type SCSF-78 (Kuraray, Japan) with double cladding and $\varnothing = 0.83$ mm outer diameter. The cladding thickness is $d_{\text{clad}} \approx 0.1$ mm, leading to a 0.73 mm thick core made of a polystyrene base with refractive index $n_{\text{core}} = 1.6$. The outer cladding is made of a fluorinated polymer with refractive index $n_{\text{clad}'} = 1.42$ and the inner cladding is made of polymethylmethacrylate with refractive index $n_{\text{clad}} = 1.49$. The emission spectrum extends from $\lambda \sim 415$ – 550 nm with a maximum at $\lambda \sim 440$ nm for fibres of short lengths. For a double cladding fibre the critical axial angle is given by $\theta_{\text{crit}} = \arccos n_{\text{clad}'}/n_{\text{core}} = 26.7^\circ$. The trapping efficiency for photons produced close to the axis of the fibre is 5.3 % giving 70 % more light than single cladding fibres, where the efficiency for light trapped inside the core is only 3.1 %.

The fibre arrays consisted of 4 double layers. A fibre column was formed by 4 fibres, one from each double layer, coupled to one common read-out channel of the photo-detector by a small plastic cookie with a matrix of holes. These columns were aligned along the incident particle direction. The read-out was one-sided by multi-anode photomultipliers (MaPMTs). No optical grease was used between fibres and the entrance window. The MaPMTs of type R7259K (Hamamatsu Photonics, Japan) are fitted with a 32-channel linear array of metal electrodes. The photocathode material is bialkali and the window is made of 1.5 mm thick borosilicate glass. The effective area per channel is 0.8×7 mm² with a pitch of 1 mm. A complication arises from the fact, that the numerical aperture for the multi-cladding fibre is 0.72, so that the light cone at the photo-cathode has a diameter of 2.32 mm. This results in a hit multiplicity of typical 3 neighbouring channels.

The MaPMTs have been characterised with an average anode luminous sensitivity of $S_a = 374$ A/lm (according to data sheet 140 A/lm is typical), an average cathode luminous sensitivity $S_c = 84$ $\mu\text{A}/\text{lm}$ (70 $\mu\text{A}/\text{lm}$ typical), and an average gain $G = 4.4 \cdot 10^6$ ($2 \cdot 10^6$ typical). The gain uniformity between anodes was found to be between 1:1.1 and 1:1.25 (1:1.5 typical), with the edge

anodes having slightly lower gains on average. Hardly any strip has less than 70% of the maximum gain of a given photomultiplier.

Instead of supplying dynode voltages through a voltage divider the MaPMTs were powered by individual Cockcroft-Walton bases (HVSys, Russia). The dc voltage is pulsed and converted with a ladder network of capacitors and diodes to higher voltages. Stiff high voltage cables are not needed, since only ~ 140 V has to be delivered to the first front-end board, where the voltage is daisy-chained to the other boards of the detector plane.

For the construction of the fibre bundles position matrices were designed, allowing for the mounting and the alignment of the fibres with the desired pitch. The construction procedure for the fibre bundles was to glue single layers of 16 fibres into grooved aluminium plates with acrylic white paint. A total of 8 single layers is needed for each bundle. These bundles were then glued into the cookies. The bundles were polished using a diamond cutting tool (Mutronic, Germany). Two of the three bundles had to be bent. This was done by placing them into an oven at a temperature of 70°C for about 1 hour and bending them into the desired shape.

As half of the scintillation light is emitted in the direction opposite to the photomultiplier, light reflected by the end face can contribute significantly to the total light output. In order to increase the light yield, some of the fibre bundles used in the tests were aluminised at the polished free end face for a high reflectivity. A vaporisation chamber was utilised that consisted of a vacuum chamber with an electric oven in which a small pellet can be placed. The aluminium coating adhered firmly and smoothly to the end face of the bundle. The increase of light yield was confirmed with a ^{90}Sr source in laboratory measurements and amounted to $\sim 50\%$.

The beam-tests at MAMI were performed with a fibre detector positioned near the focal plane of a large magnetic spectrometer where scattered electrons have an inclination of 45° with respect to the normal to the detection plane. If the particles were crossing the fibre array with an angle to the column direction its tracking capability would be compromised. Accordingly, two bundles of 4 double layers with the fibre columns following the 45° inclination in square packing geometry were built. The fibre array has an overlap of $o = \varnothing(1 - 1/\sqrt{2}) \approx 0.24$ mm, and a column pitch of $p = \varnothing/\sqrt{2} \approx 0.59$ mm, see Fig. 1. Our experience shows that the best way to stack the fibres during the actual assembly is layer-by-layer. Other sequences may cause sizeable misalignments which directly lead to errors in the position determination.

For the tests in the carbon beam 3 bundles of 128 fibres each with an active area of 150×20 mm² were constructed in a square packing geometry of 4 double layers, see Fig. 2. Overlap and column pitch of this geometry are identical to

the 45° geometry. Results from laboratory measurements with a ^{90}Sr source resulted in a light yield of 4–5 photoelectrons per pixel with a multiplicity of 3 pixels, corresponding to 15 photoelectrons per crossing minimum ionising particle.

In the KAOS/A1 spectrometer, particles will cross the electron arm focal plane with an inclination angle of $50 - 70^\circ$ with respect to the normal of the plane. Regarding this geometry fibre arrays with a hexagonal packing of slanted columns with 60° inclination were constructed, see Fig. 3. Overlap and column pitch of this geometry are 0.41 mm. These detectors were tested in the beams at GSI.

A 12-layer front-end board able to accommodate the three MaPMTs was developed by the Institut für Kernphysik for this type of fibre detector. It supplies the voltage for the Cockcroft-Walton voltage multipliers and brings the analogue signals along equalised conducting paths to the RJ-45 connectors for the output to the discriminators. For amplitude-compensated timing two 32-channel discriminator boards, custom designed and built by the Institut für Kernphysik, each with 4 integrated low-walk double threshold discriminators (DTDs), were used. The DTD boards were placed in an 6U crate together with a controller board. The communication with a PC was done via parallel port. The time is picked off by CATCH cards, developed for the COMPASS collaboration [11]. At GSI analogue output boards with $50\ \Omega$ coaxial connectors were attached to the discriminator boards to access also the pulse heights of each channel. The pulse height information of 22 channels was read out by two Model 2249A CAMAC ADCs (LeCroy, US). The ADCs offer a resolution of 10 bits at an input sensitivity of $0.25\ \text{pC}/\text{count}$.

The trigger was either derived from the second plane of the fibre detector or from a reference counter, a scintillation paddle that was installed 2 m upstream in the beam-line. The time difference between individual channels and the reference counter showed a dependence on the pulse height. This time walk effect was corrected according to the equation $\Delta t_c = \Delta t - c_{\text{walk}}/\sqrt{Q}$, where c_{walk} is a global correction coefficient and Q the charge of the signal as measured by the ADC. Any time jitter from the reference counter drops out when the residual time between two detector planes is determined.

3 Performance of a fibre detector with electrons at the Mainz microtron MAMI

In order to measure the tracks of electrons through a 32-channel fibre detector, it was placed inside the heavy shielding house of spectrometer A, a large high-resolution magnetic spectrometer at the Mainz Microtron MAMI [12]. The

focal plane of the spectrometer A has a length of approximately 2 m, and it is inclined at an angle of 45° to the reference particle trajectory. The divergence of the particle trajectories is about 24° . The fibre detector was sandwiched between the drift chambers and the scintillator paddles of the focal plane detector system.

Two vertical drift chambers (VDCs) measure the dispersive coordinate x plus the corresponding angle θ and the non-dispersive coordinate y plus the angle ϕ . The electron hit position was found by extrapolating the reconstructed track from the focal plane to the fibre detector. Fig. 4 (left) shows the geometrical acceptance covered by the fibre detector inside the spectrometer, determined by such an extrapolation. The kinematics of the reaction was chosen so that the particle illumination was homogeneous over the fibre detector.

The hit multiplicity of the detector was relatively high, $N \approx 4$, the main reason being a large optical cross-talk in the MaPMT. A simple estimator for the x -position of the form $x = \sum_{i=1}^N x_i / N$ was used accordingly, where x_i was the parametrised geometrical centre position of the i th channel and N the hit multiplicity. This track estimate was compared to the track reconstructed from the VDCs and projected onto the detector base coordinate, see Fig. 4 (right). Small non-linearities at the edges of the diagonal line indicate that better estimators based on weighted averages were needed. A detailed analysis of the correlation revealed a few misalignments in the fibre bundles caused by the demanding construction of the 45° geometry. Fig. 5 (left) shows the residual of track position defined as the difference between the position reconstructed by the VDCs and the position measured by the fibre detector. A width of FWHM ~ 1.1 mm can be deduced from the distribution. It is assumed that the resolution of the VDC, $\Delta x < 100 \mu\text{m}$ for the dispersive coordinate, was high compared to the fibre detector.

The trigger detectors of the spectrometer consist of two segmented planes of plastic scintillation detectors. The arrival time of the electrons was measured in the fibre detector with respect to the following two overlapping paddles. Fig. 5 (right) shows the time spectra obtained from the coincidence timing with the trigger scintillators before and after performing the walk correction for the paddles and the calibration of the channel-to-channel variations of the fibre detector. The combined resolution of FWHM ≈ 1 ns was rather good for the small amount of light from the fibres.

The detection efficiency was determined by sandwiching the fibre detector between the VDC and the scintillators, and using the three-detector method. It was found to be 99% independent of the threshold.

4 Performance of a fibre detector in a carbon at GSI

In Cave C of GSI tests of a fibre detector with three bundles in a ^{12}C beam of 2 AGeV energy were performed. Two bundles of the detector were aligned to a single plane, and one bundle formed a parallel plane directly behind.

In deducing the time resolution, an iteration over all hits in a plane including multiple hits in a channel was performed, and clusters of correlated hit times were searched for. The cluster with the time closest to the trigger signal time was retained, and within the cluster the time of the first arrived signal was chosen as hit time. In the algorithm a minimum time separation of 10 ns between clusters and a hit in a coincidence window of 20 ns width were required. A time walk correction for the hit times was not needed. The hit time residual, defined as the difference between the two hit times in the two planes of fibres, was distributed with a width of $\text{FWHM} = 330 \text{ ps}$ for the carbon beam, see Fig. 6. No significant dependence of the time resolution on photomultiplier high voltage was observed. The time resolution of a single detector plane was derived to be $\text{FWHM} \sim 330 \text{ ps}/\sqrt{2} = 230 \text{ ps}$.

The pulse height spectra for different high voltages (-650 , -700 , and -850 V) were fitted to get the normalisation, A_i , and the pedestal position, p_i , for each ADC channel i . With these calibration values the spectra were corrected for channel-to-channel gain variations. For 11 neighbouring channels in one plane and the same number of channels in the plane directly behind the pulse height information was available, and the hit channel was determined by the pulse height maximum. To validate the assignment the centroid of charges of up to five channels was determined. Fig. 7 shows the correlation between the centroids of charges in both detector planes. The steps are a consequence of the discretisation in fibre channels and appear with a pitch of $\Delta c_A, \Delta c_B \approx 0.6 \text{ mm}$. Taking the centroid of only a limited number of hit channels proved to be superior to the centroid of all hit channels. The algorithm was applied to the central area of the detector away from the edges, where the number of channels available for the averaging is restricted. The hit position residual, defined as the difference between the two track position estimates in the two planes of fibres, was measured with a $\text{FWHM} \sim 0.27 \text{ mm}$, see Fig. 8. This accuracy was sufficient for an unambiguous identification of the hit channel, leading to a spatial accuracy of $0.6 \text{ mm}/\sqrt{12} \approx 170 \mu\text{m}$ (rms). In principle, the resolution can be improved by distinguishing between hits in the overlap region of two neighbouring channels from central hits. An analysis, which required a minimum charge drop of 10% compared to the neighbours was performed. The identification of the hit channel was then improved and the identification of overlapping channels became possible, but a large optical cross-talk interferes with such a requirement. The channel with the pulse height maximum was strongly correlated to the hit time defining channel showing that

ADC calibration constants and TDC off-set values had both been correctly determined.

It is worth estimating the spatial accuracy of the fibre detector for set-ups without analogue read-out. Cross-talk between neighbouring channels then perturbs the reconstruction of the position of the track position by causing finite hit multiplicity. Since no absolute position of the particle tracks were known, one has to compare the hit channel mean value with the estimated position using the ADC information which is assumed to be more accurate. The difference of the hit channel mean value as a simple estimate of track position and the reconstructed position was evaluated by requiring a certain minimum ADC value (typically 70% of the maximum) to mimic a given discriminator voltage threshold. This difference still includes contributions from the uncertainties in both position estimators and the granularity of the fibre array. The distributions were measured with an average $\langle \text{FWHM} \rangle \sim 0.6$ mm (approx. the fibre pitch), an average $\langle \text{RMS} \rangle$ of 0.5 mm, and an average $\langle \text{FWTM} \rangle < 1$ mm.

The pulse height distribution of a typical detector channel (B 24) is shown in Fig. 9 (left). The appearance of a series of peaks below the maximum pulse height at ADC channel ~ 100 was caused by the spread of secondary electrons and the cross-talk between channels that transport a fixed fraction of the signal into neighbouring channels. The hit multiplicity of one detector plane is shown in Fig. 9 (right). For a high voltage of -650 V the mean value of the distribution was $N \sim 5$, increasing with higher voltages. The overall photo-multiplier gain increased by a factor ~ 2 between -650 V and -850 V. From the distributions of the pulse height sum over all channels a relative energy resolution of $\Delta E/E = 15\text{--}20\%$ was determined. The detection efficiency of a plane, i.e. the probability to find at least one hit in one plane provided a hit in the other plane, was above 99 %.

5 Performance of a fibre detector in a beam of different particle species at GSI

A fibre detector in Cave A of GSI was tested in a $p/\pi^+/d$ beam of 3.3 Tm magnetic rigidity with dominant protons of 1 GeV/c momentum as well as in a carbon beam of 2 AGeV energy.

The hit time residual was measured with a width of 720 ps for the beam of different particle species, see Fig. 10. The time resolution of a single detector plane was derived to be $\text{FWHM} \sim 310 \text{ ps}/\sqrt{2} = 220$ ps for the carbon beam and 510 ps for the beam of different particle species. For the measurements in the carbon beam the high voltages were reduced from -850 V to -600 V to compensate for the large pulse heights due to the large energy deposit. Of

course, statistical fluctuations in the number of detected photons were not affected by this reduction of the gain.

The multiplicity distributions of both detector planes and are shown in Fig. 11 with average values close to $N = 5$ channels. These values are the consequence of some small misalignment and mainly cross-talk in the glass window of the MaPMT. By using the pulse height information the hit channel was determined as the centroid of charges. The hit position residual, defined as the difference between the two estimates in the two planes of fibres, was fitted with a width of $\text{FWHM} = 0.46$ mm for the beam of different particle species. It was to some extent compromised by gain variations.

The energy response of the fibre detector was studied in the beam of different particle species. Fig. 12 (top) shows the distribution of the pulse height sum over neighbouring channels of one detection plane. From the Gaussian fit to the data a relative variation in the measured energy deposition, $\Delta E/E$, of 60% was derived for the dominant particle species. Fig. 12 (bottom) shows the energy loss vs. relative time-of-flight, in which dominant protons and sub-dominant π^+ , deuteron, and ^3He were separated.

6 Concluding remarks

The performance of scintillating fibre detectors with MaPMTs was extensively tested using electrons at the spectrometer facility at MAMI, ^{12}C ions of 2 AGeV energy as well as $p/\pi^+/d$ particles at GSI. The hit position was reconstructed by calculating the centroids of the charges collected from each read-out channel. Good spatial accuracy and time resolution were obtained at practically unity detection efficiency. The energy response to different particle species was studied.

During tests at MAMI and at GSI the optical cross-talk caused by the finite thickness of the PMT entrance window could be verified. Indeed, this behaviour of the PMT has been also recognised by Hamamatsu. Only very recently, a 32-channel PMT with black shielding lamellae embedded in the glass window became commercially available with significantly reduced cross-talk.

It is currently planned to perform in 2009 a first HypHI experiment at GSI using three arrays of scintillating fibres as well as a first KAOS/A1 experiment on the electro-production of hypernuclei at MAMI with fibre detectors in the spectrometer's electron arm.

Acknowledgements

Work supported in part by Bundesministerium für Bildung und Forschung (bmb+f) under contract no. 06MZ176. T.R. Saito and his research group are granted by the Helmholtz Association and GSI as Helmholtz-University Young Investigators Group VH-NG-239 and DFG research grant SA 1696-1/1.

References

- [1] J. Bähr, et al., Nucl. Instr. and Meth. in Phys. Res. A348 (1994) 713–718.
- [2] F. Bosi, et al., Nucl. Instr. and Meth. in Phys. Res. A374 (1996) 48–56.
- [3] S. Horikawa, et al., Nucl. Instr. and Meth. in Phys. Res. A516 (2004) 34–49.
- [4] P. Achenbach, et al., Performance of a fibre detector at a ^{12}C beam of 2 AGeV energy, GSI Sci. Report 2006, GSI, Darmstadt (2007), p. 224.
- [5] P. Achenbach, et al., Particle identification with a fibre detector in a $p/\pi^+/d$ cocktail beam of 3.3 Tm magnetic rigidity at GSI, GSI Sci. Report 2007, GSI, Darmstadt (2008).
- [6] P. Achenbach, Probing hypernuclei at $\bar{\text{P}}\text{anda}$ and at MAMI-C, in: J. Pochodzalla, Th. Walcher (Eds.), Proc. of the IX. Intern. Conf. on Hypernuclear and Strange Particle Physics, Joh. Gutenberg-Univ., Mainz, 10–14 Oct. 2006, Springer, 2007, pp. 79–84.
- [7] P. Achenbach, et al., New detectors for the kaon and hypernuclear experiments with KAOS at MAMI and with PANDA at GSI, in: V. Luth (Ed.), Proc. of the IX. Intern. Symposium on Detectors for Particle, Astroparticle and Synchrotron Radiation Experiments, SLAC, 3–6 April 2006, eConf C0604032, 2006, p. 144.
- [8] T. R. Saito, et al., The HypHI project at GSI and FAIR, in: J. Pochodzalla, Th. Walcher (Eds.), Proc. of the IX. Intern. Conf. on Hypernuclear and Strange Particle Physics, Joh. Gutenberg-Univ., Mainz, 10–14 Oct. 2006, Springer, 2007, pp. 171–176.
- [9] O. Lepyoshkina, et al., Scintillating fiber detector for the HypHI phase 0 experiment, GSI Sci. Report 2006, GSI, Darmstadt (2007), p. 223.
- [10] D. Nakajima, et al., Scintillating fiber detectors for phase 0 experiment of HypHI project, GSI Sci. Report 2007, GSI, Darmstadt (2008).
- [11] H. Fischer, et al., Nucl. Instr. and Meth. in Phys. Res. A461 (2001) 508–510.
- [12] K. I. Blomqvist, et al., Nucl. Instr. and Meth. in Phys. Res. A403 (1998) 263–301.

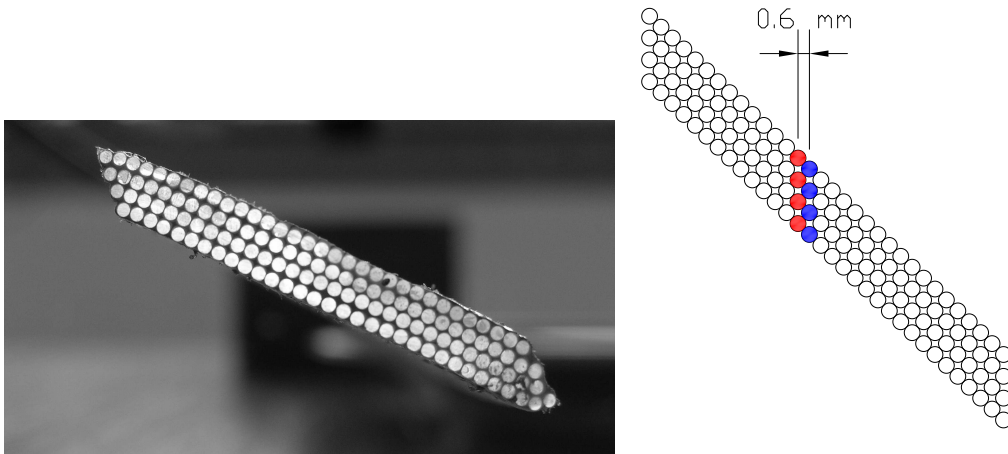


Fig. 1. Scheme of a 45° column angle geometry with 4 double layers of fibres and a column pitch of 0.6 mm and an overlap of 0.24 mm (right). A photograph of an assembled fibre bundle (left).

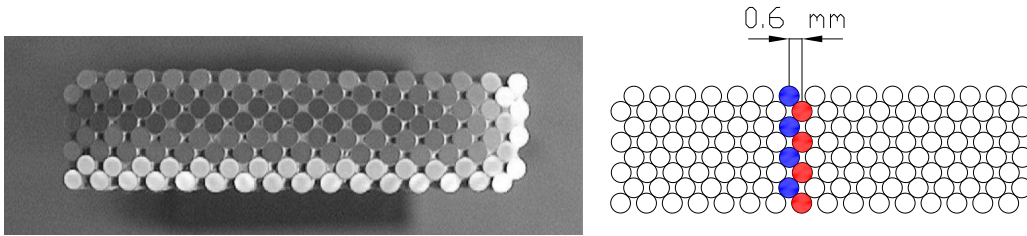


Fig. 2. Scheme of a 0° column angle geometry with 4 double layers of fibres and a column pitch of 0.6 mm and an overlap of 0.24 mm (right). A photograph of an assembled fibre bundle (left).

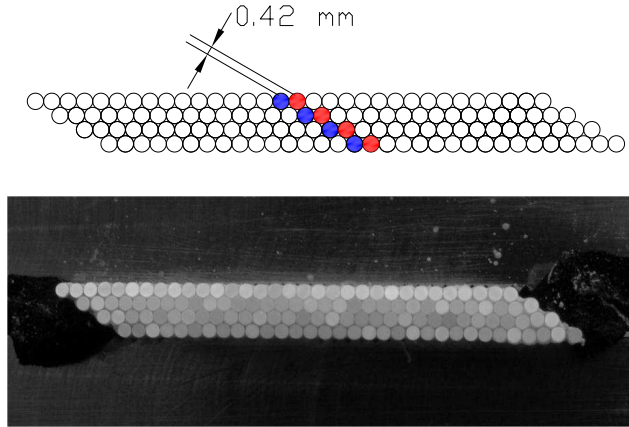


Fig. 3. Scheme of a 60° column angle geometry with 4 double layers of fibres and a column pitch of 0.42 mm and an overlap of 0.42 mm (top). A photograph of an assembled fibre bundle (bottom).

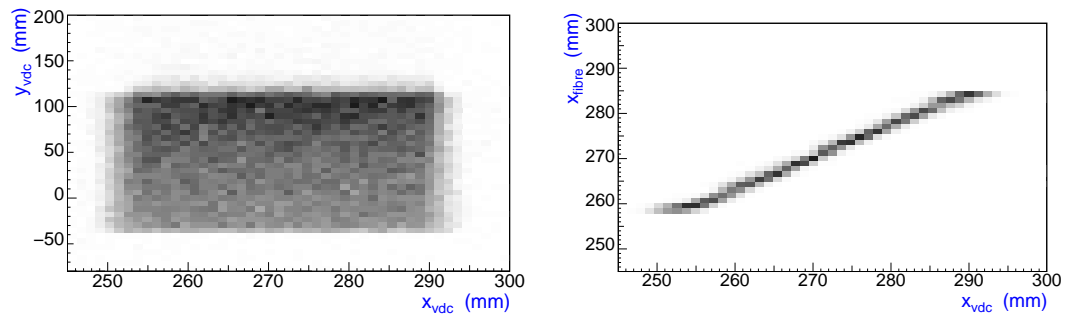


Fig. 4. Geometrical acceptance covered by the fibre detector inside the spectrometer shown by the track positions reconstructed with the vertical drift chambers (left). The reconstructed position projected onto the base coordinate versus the measured position obtained from the fibre detector with a simple estimator (right).

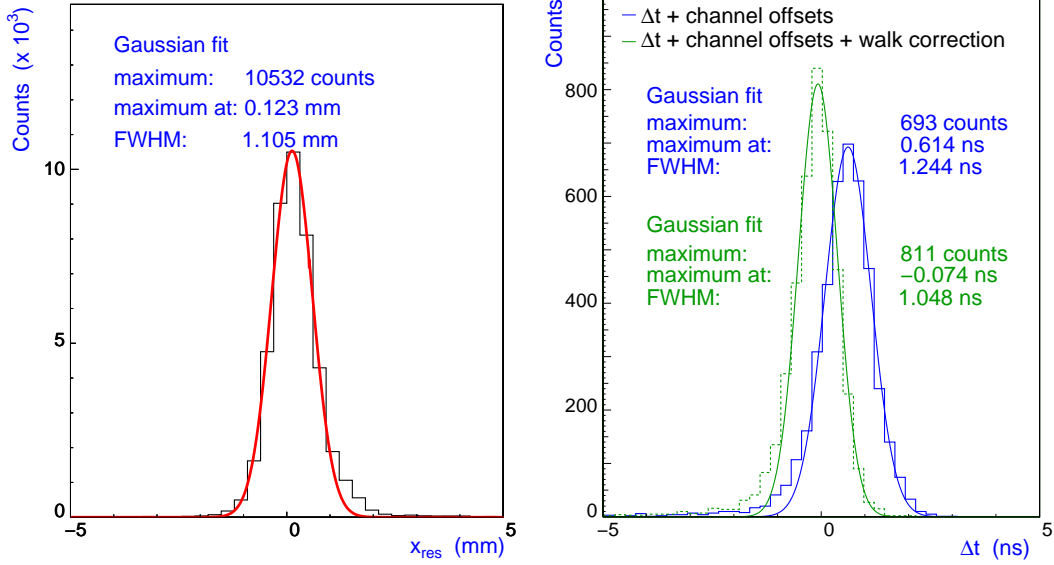


Fig. 5. The residual of track position obtained from the drift chamber track reconstruction and the simple estimator for the fibre detector (left). The residual of hit times obtained from the trigger scintillators and the fibre detector before and after walk correction for the trigger and calibration of the fibre channel-to-channel variations (right).

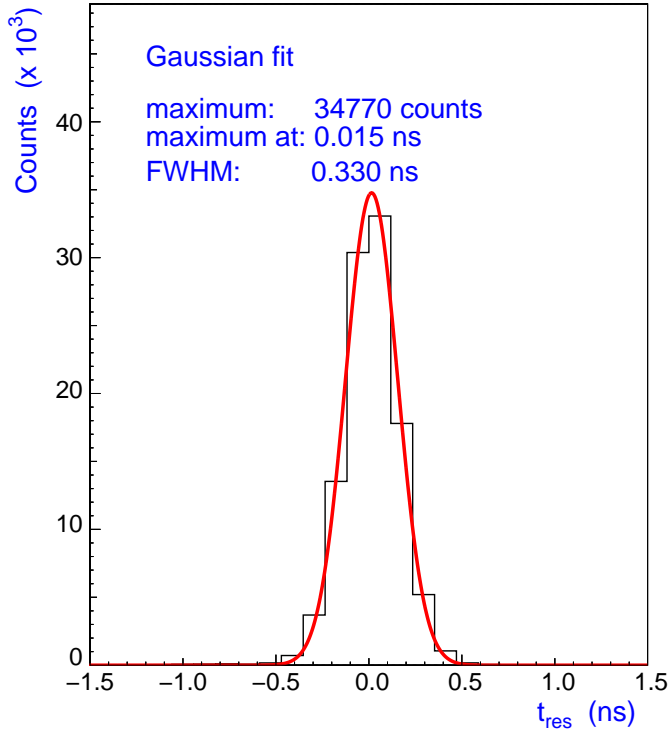


Fig. 6. The residual of hit times between two detector planes, $t_A - t_B$. A Gaussian fit is shown providing a width of $\text{FWHM} = 330$ ps. The time resolution of a single detector plane was derived to be $\text{FWHM} \sim 330 \text{ ps}/\sqrt{2} = 230$ ps.

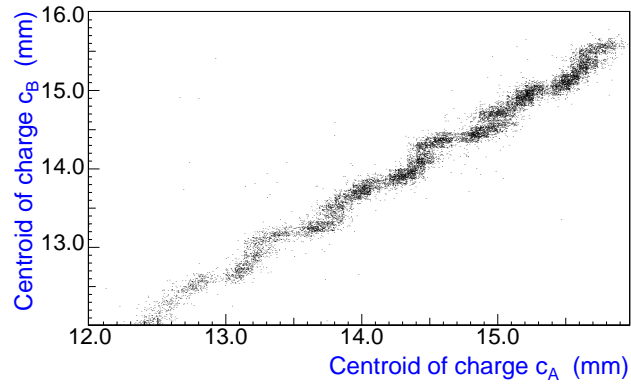


Fig. 7. Scatter plot showing the correlation between the centroids of charges in both detector planes. The steps appear with a pitch of $\Delta c_A, \Delta c_B \approx 0.6$ mm.

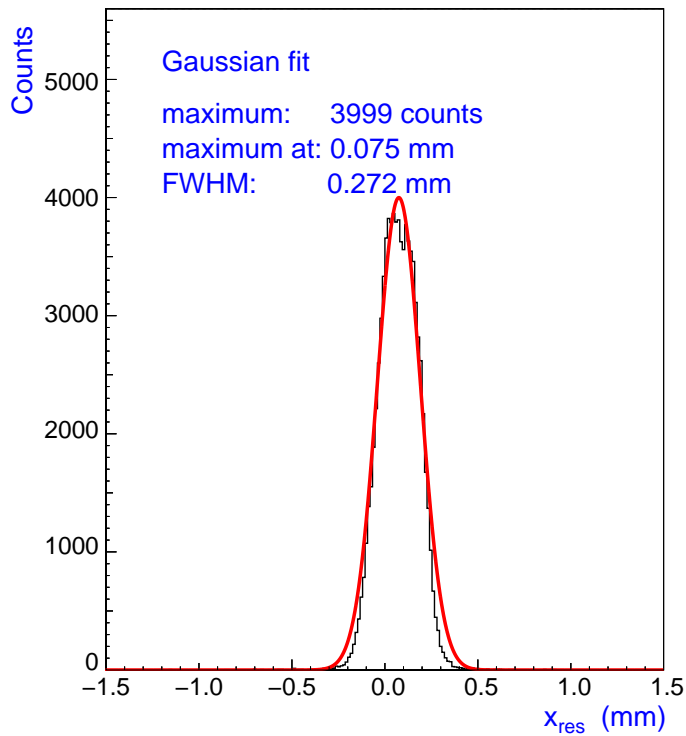


Fig. 8. The residual of track position estimates between both detector planes, $x_A - x_B$, using the centroid of charges. A Gaussian fit is shown providing a width of $\text{FWHM} = 0.27$ mm, however, the distribution is non-Gaussian with two overlapping peaks because of the discretisation in fibre channels.

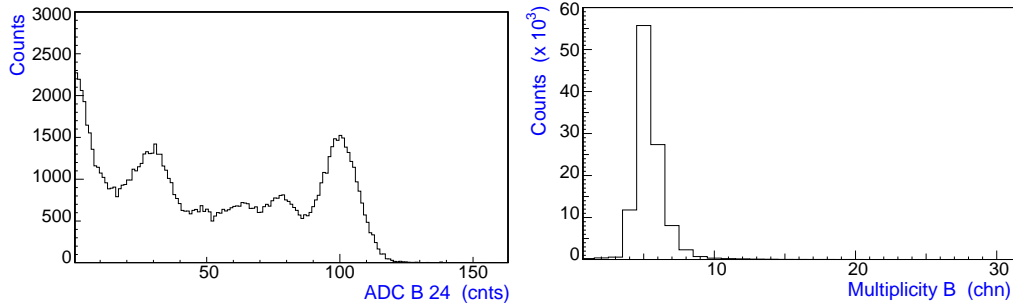


Fig. 9. Pulse height distribution of a typical detector channel (left). Distribution of hit multiplicities in the corresponding detector plane (right), which causes the series of peaks in the pulse height distribution.

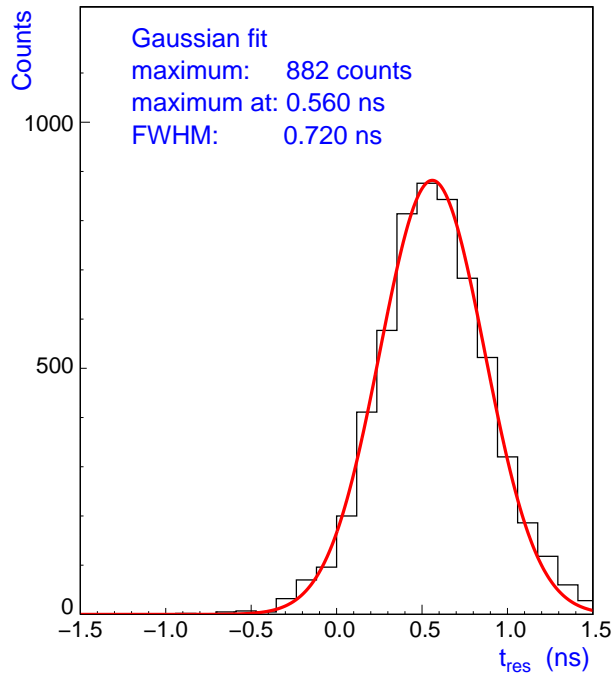


Fig. 10. The residual of hit times between two detector planes, $t_A - t_B$. A Gaussian fit is shown providing a width of $\text{FWHM} = 720$ ps for the beam of different particle species. The time resolution of a single detector plane was derived to be $\text{FWHM} \sim 510$ ps.

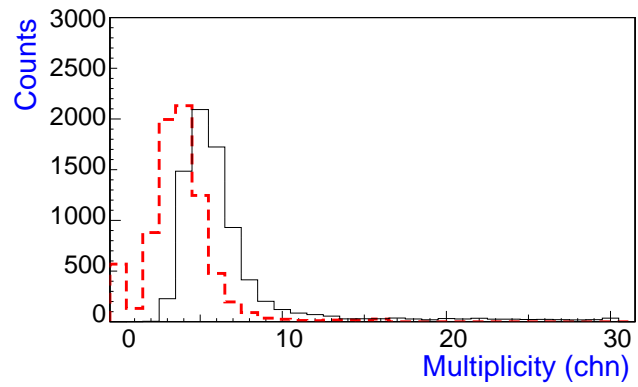


Fig. 11. The hit multiplicities of both detector planes for the beam of different particle species. The trigger was provided by the plane represented with the dashed curve.

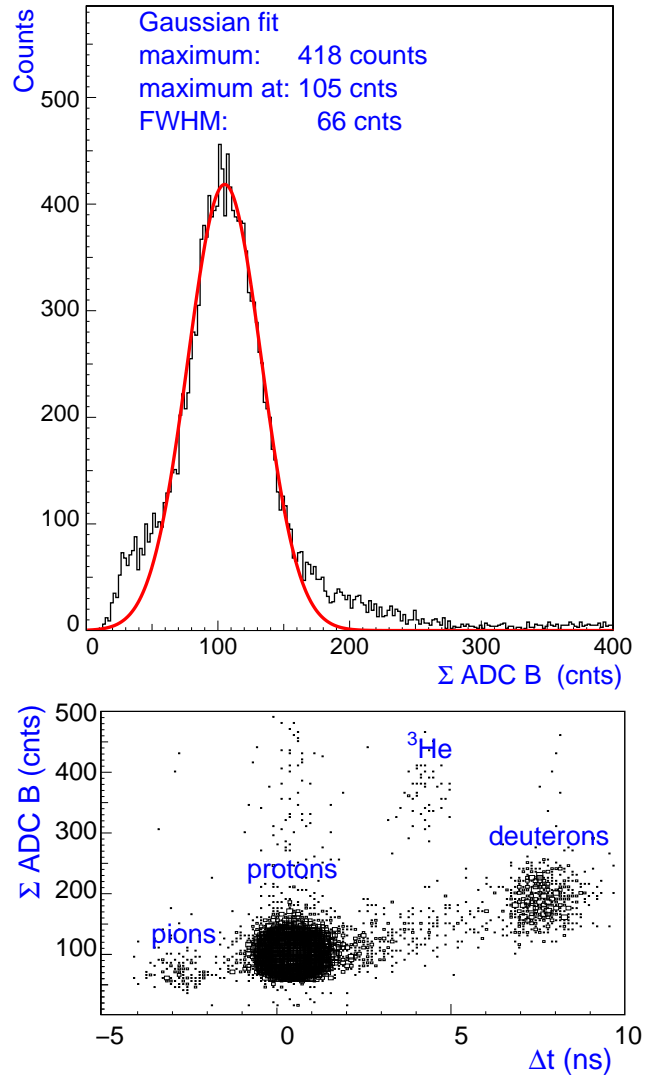


Fig. 12. Distributions of the pulse height sum over all channels of one detector plane for the beam of different particle species (top). From the Gaussian fit to the proton peak a relative energy resolution $\Delta E/E \sim 60\%$ was derived. The pulse height sum is shown vs. the time-of-flight so that π^+ , proton, deuteron, and ^3He were separated (bottom).